Birkbeck
UNIVERSITY OF LONDON

BIROn - Birkbeck Institutional Research Online

Crawford, Ian and Lallement, R. and Price, R.J. and Sfeir, D.M. and Wakker, B.P. and Welsh, B.Y. (2002) High-resolution observations of interstellar Na I and Ca II towards the southern opening of the 'Local Interstellar Chimney': probing the disc—halo connection. Monthly Notices of the Royal Astronomical Society 337 (2), pp. 720-730. ISSN 0035-8711.

Downloaded from: http://eprints.bbk.ac.uk/id/eprint/28516/

Usage Guidelines:
Please refer to usage guidelines at https://eprints.bbk.ac.uk/policies.html or alternatively contact lib-eprints@bbk.ac.uk.

Mon. Not. R. Astron. Soc. **337,** 720–730 (2002)

High-resolution observations of interstellar Na I and Ca II towards the southern opening of the 'Local Interstellar Chimney': probing the disc–halo connection

I. A. Crawford,[1⋆] R. Lallement,[2] R. J. Price,[1] D. M. Sfeir,[3,4]
B. P. Wakker[5] and B. Y. Welsh[3]

[1]*Department of Physics and Astronomy, University College London, Gower Street, London WC1E 6BT*
[2]*Service d'Aéronomie du CNRS, BP 3, 91371 Verrieres-le-Buisson, France*
[3]*Space Sciences Laboratory, University of California, Berkeley, CA 94720, USA*
[4]*Department of Aerospace and Mechanical Engineering, University of Southern California, Los Angeles, CA 90089, USA*
[5]*Department of Astronomy, University of Wisconsin, 475 N. Charter Street, Madison, WI 53706, USA*

Accepted 2002 August 9. Received 2002 August 7; in original form 2002 July 12

ABSTRACT

We present high-resolution ($R = 400\,000$) observations of interstellar Ca II and Na I absorption lines towards seven stars in the direction of the southern opening of the recently identified Local Interstellar Chimney. These lines of sight probe the lower Galactic halo ($0.3 \lesssim |z| \lesssim 2.5$ kpc), without the complication of sampling dense foreground interstellar material. In addition to components with velocities expected from Galactic rotation, these stars also exhibit components with negative local standard of rest velocities, which are contrary to the sense of Galactic rotation for the sightlines observed. After a discussion of possible origins for these peculiar velocities, we conclude that at least some of them result from gas falling towards the Galactic plane from distances of $|z| \gtrsim 300$ pc. The narrow linewidths are generally inconsistent with temperatures as high as the ∼6000 K generally assumed for the so-called Lockman layer. Rather, the picture that emerges is one of a scattered, generally infalling, population of high-$|z|$ diffuse clouds, seemingly not very different from those encountered in the local interstellar medium. Overall, we argue that our results are most consistent with a 'Galactic fountain' model.

Key words: ISM: structure – Galaxy: halo.

1 INTRODUCTION

As part of an on-going programme to explore the structure of the local interstellar medium by means of high-resolution absorption-line spectroscopy (e.g. Crawford, Craig & Welsh 1997; Crawford, Lallement & Welsh 1998), we report here on a study of interstellar Ca II K and Na I D lines towards seven stars situated in the lower Galactic halo ($0.3 \lesssim |z| \lesssim 2.5$ kpc). Our aim is to study the physical and kinematical state of matter in the lower halo, and its relationship to more local interstellar structures in the solar vicinity.

It is generally accepted (e.g. Cox & Reynolds 1987; Frisch 1995), that the Sun is situated within a hot ($T \sim 10^6$ K), low-density ($n_{\rm H} \sim 0.005$ cm^{-3}) region known as the local bubble (LB). Recently, Sfeir et al. (1999) have conducted a preliminary survey of Na I absorption within 300 pc of the Sun, and revealed the presence of an absorption boundary (or 'wall') of cold, and relatively dense [N(H I) > 5×10^{19} cm^{-2}] neutral gas surrounding the LB at distances from the Sun varying between 65 and 250 pc. This neutral boundary of the LB is found to be well defined in the Galactic plane, but at high Galactic latitudes the LB appears to be open-ended in both hemispheres with no well-defined dense neutral absorption boundary. This 'Local Interstellar Chimney' (a term first coined by Welsh et al. 1999) is found to point towards $l = 155°$, $b = +58°$, to extend at least to $|z| \approx 200$ pc and to be tilted perpendicularly to the plane of Gould's Belt. The presence of this open-ended structure provides a unique opportunity to probe the structure of the inner halo region by means of high-resolution measurements of interstellar absorption lines that are essentially free from the interference of dense foreground clouds.

The neutral inner halo is thought to consist of a confined, cool ($T \lesssim 500$ K) component with an exponential scaleheight of ∼100 pc (where the interstellar medium largely forms discrete clouds), and

⋆E-mail: iac@star.ucl.ac.uk

© 2002 RAS

Downloaded from https://academic.oup.com/mnras/article-abstract/337/2/720/1026619 by Birkbeck College, University of London user on 12 August 2019

an extended, more rarefied warm ($T \sim 6000$ K; e.g. Spitzer & Fitzpatrick 1993) diffuse component with an estimated scaleheight of ~500 pc (the so-called 'Lockman layer'; Lockman 1984; Lockman, Hobbs & Shull 1986). Although the latter was originally envisaged as a smooth distribution of 'intercloud' type material (Lockman et al. 1986), more recent work suggests an interpretation where the whole H I layer consists of essentially discrete clouds, the individual motions of which support its vertical extent against the Galactic gravitational potential (Lockman & Gehman 1991 and references therein). This latter interpretation is supported by the extensive survey of Albert et al. (1993), which found evidence for discrete clouds (as mapped by Ca II and Ti II absorption lines) at distances $\gtrsim$1 kpc above and below the plane.

Further away from the Galactic disc the halo gas is thought to be highly ionized (the so-called 'Reynolds layer', Reynolds 1997 and references therein; see also de Boer 1998), although the proposed 1-kpc scaleheight sits uncomfortably with the apparent detection of discrete, presumably largely neutral, clouds at and beyond this distance from the plane by Albert et al. (1993). Moreover, given the existence of this ionized component, it is still uncertain whether the hot ionized gas is being advected from the disc into the halo by a Galactic 'fountain' fed by supernovae and/or bursting superbubbles in the disc (Shapiro & Field 1976; Spitzer 1990), or whether it is being heated and/or ionized by a variety of processes such as photoionization by extra-Galactic background radiation (Bregman & Harrington 1986).

Although much information already exists concerning the distribution of both high and low ionization ultraviolet (UV) and visible absorption lines in the halo (Danly 1989; Albert et al. 1993; Savage & Sembach 1996), these selections of halo lines of sight have generally been made without detailed knowledge of the intervening absorption at the LB neutral boundary. Moreover, these earlier studies have usually employed only moderate spectral resolution ($R \approx 50\,000$ or 6 km s^{-1} FWHM), making it difficult to interpret the velocity structure and observed linewidths. Here, we have circumvented the first limitation by observing stars towards the southern opening of the relatively unobscured Local Interstellar Chimney, and the second by employing a spectral resolution almost an order of magnitude higher than employed in previous studies (this improvement will be made clear by comparing our Fig. 1, with the relevant panels of fig. 2 of Albert et al. 1993).

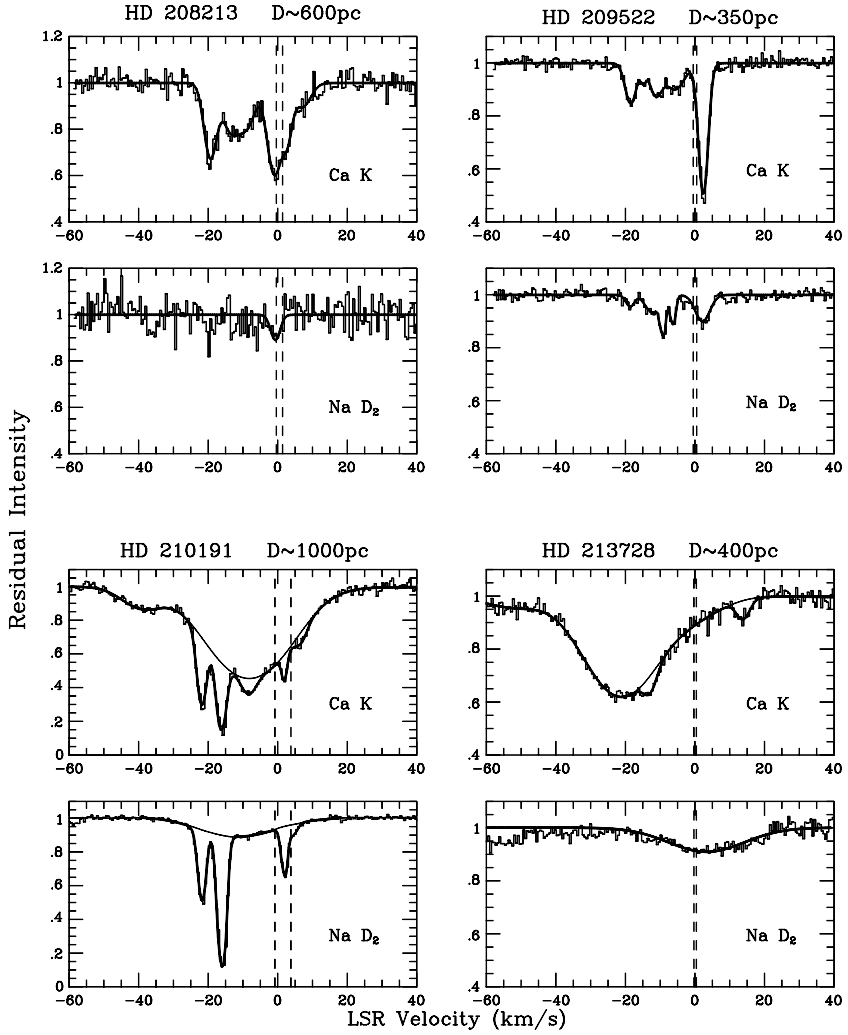

Figure 1. The interstellar Ca K and Na D_2 lines towards the observed stars. The observed data are plotted as histograms, and the best-fitting theoretical line profiles (Table 2) are shown superimposed. The smooth, broad curves indicate the adopted fits to the stellar photospheric lines where these are present. The vertical dashed lines indicate the velocity range expected to result from Galactic rotation towards each star (see the text for details).

Downloaded from https://academic.oup.com/mnras/article-abstract/337/2/720/1026619 by Birkbeck College, University of London user on 12 August 2019

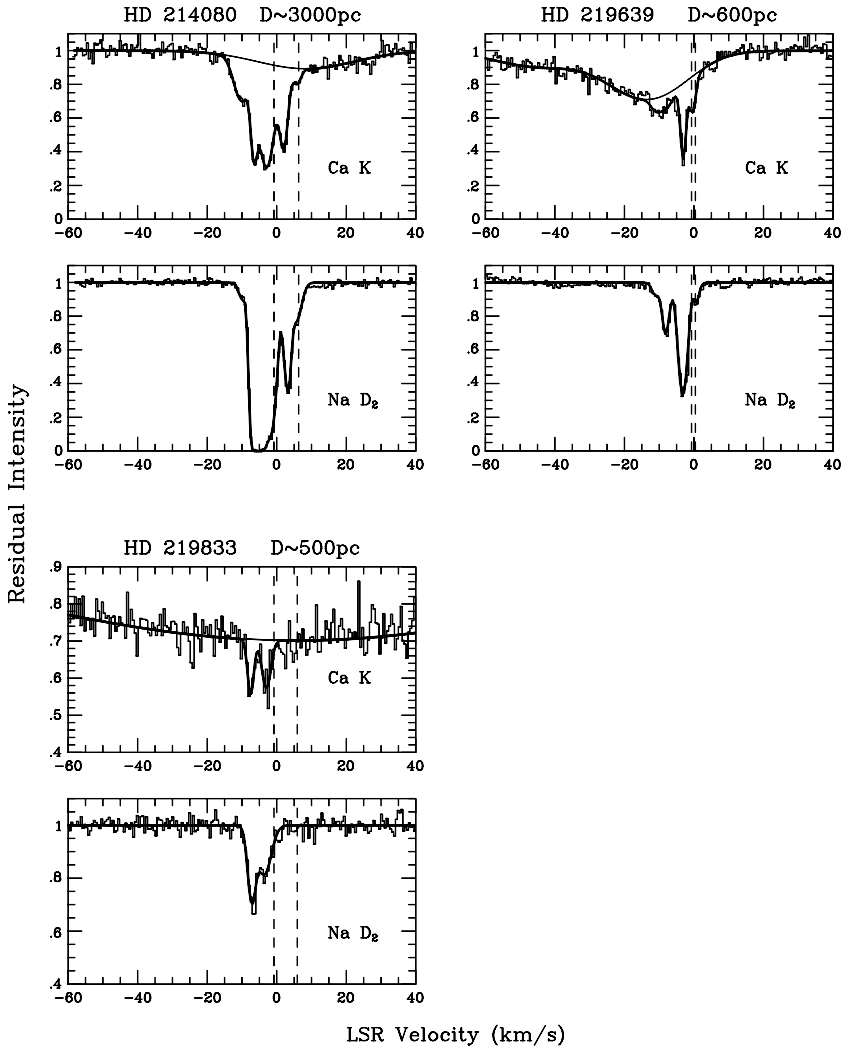

Figure 1 – *continued*

2 OBSERVATIONS AND DATA ANALYSIS

The observations were obtained using the Ultra-High-Resolution Facility (UHRF; Diego et al. 1995), at the Anglo-Australian Telescope on the nights of 2000 August 16 and 17. The spectrograph was used in its '$R = 300\,000$' mode; as discussed by Diego et al. (1995), the actual resolving power of this mode is actually somewhat higher, and measurement of the instrumental profile (using a stabilized He–Ne laser as a source) yielded a FWHM of 0.75 ± 0.01 km s^{-1}, or $R = 400\,000$. The detector was the AAO Tectronix charge-coupled device (CCD) (1024×1024 24-μm pixels). The spectrograph was used in conjunction with an image-slicer (Diego 1993), and the output was binned by a factor of 8 perpendicular to the dispersion direction to reduce the readout noise associated with the broad spectrum that results. Details of individual exposures are given in Table 1.

The spectra were extracted from the CCD images using the FIGARO data reduction package (Shortridge et al. 1998) at the UCL Starlink node, and most of the subsequent measurements were performed using the DIPSO spectral analysis program (Howarth et al. 1998). Wavelength calibration was achieved using a Th–Ar comparison lamp; second-order polynomial fits to five (Ca region) and six (Na region) comparison lines yielded rms residuals of $\lesssim$0.001 Å. Once wavelength calibrated the spectra were converted to a velocity scale relative to the local standard of rest (LSR), and are shown in Fig. 1. Several of these stars were found to exhibit photospheric Ca K and Na D lines. In addition, the 3933.29-Å line of S II occurs in the Ca K spectral region (see, e.g., Crawford 1990) and this line, off-set by -28 km s^{-1} with respect to Ca K, was found to be detectable towards three stars (HD 210191, 213728 and 219639). These relatively broad stellar lines form the local continua for the interstellar lines, and are clearly visible in Fig. 1.

The interstellar line profiles were fitted using a least-squares minimization (Levenberg–Marquardt) algorithm, developed within the IGOR-PRO software environment (a WaveMetrics Inc. product). The wavelengths and oscillator strengths were taken from Morton (1991), and the hyperfine structure in the Na lines (see, for example, Welty, Hobbs & Kulkarni 1994) was included in the line profile analysis. In the case of Na I, simultaneous fits were performed to both the D_2 and D_1 lines, although for reasons of space only the former are plotted in Fig. 1. Telluric lines caused by water vapour were removed by dividing each spectrum by a theoretical atmospheric transmission spectrum, calculated by adjusting the water vapour column density to the observing conditions (Lallement et al. 1993). The resulting line profile fits are characterized by a LSR radial velocity ($v_{\rm LSR}$), line-of-sight velocity

Downloaded from https://academic.oup.com/mnras/article-abstract/337/2/720/1026619 by Birkbeck College, University of London user on 12 August 2019

Table 1. List of stellar and observational data. The visual magnitudes (V), spectral types, and Galactic coordinates (l, b) are taken from the SIMBAD data base. (The question mark for the spectral type of HD 210191 flags an uncertainty discussed in Section 3). E_{B-V} is the colour excess, calculated from the observed colours and the intrinsic colours listed by Schmidt-Kaler (1982); $D_{\rm Hipp}$ and $D_{\rm phot}$ are the *Hipparcos* trigonometric (ESA 1997) and photometric distances, respectively, both rounded to the nearest two significant figures (the photometric distances assume the absolute magnitudes given by Schmidt-Kaler 1982). W_λ(Ca K) and W_λ(Na D_2) are the total interstellar Ca K and Na D_2 equivalent widths, respectively. The last two columns indicate the number and length of integrations made in each spectral region.

Star (HD)	V	Sp. Type	l	b	$D_{\rm Hipp}$ (pc)	$D_{\rm phot}$ (pc)	E_{B-V}	W_λ(Ca K) (mÅ)	W_λ(Na D_2) (mÅ)	Exp. (Ca II) ($n \times$ s)	Exp. (Na I) ($n \times$ s)
208213	8.5	B3 Vn	17.90	−51.47	610^{+1100}_{-240}	1010	0.04	94 ± 4	7 ± 4	2×1800	1×1800
209522	6.0	B4 IVne	23.58	−53.01	350^{+120}_{-70}	390	0.04	50 ± 2	32 ± 2	1×1200	2×1200
210191	5.8	B2 III ?	37.15	−51.76	$2100^{+\infty}_{-1400}$	770	0.08	83 ± 2	102 ± 2	2×1200	1×1800
213728	6.7	B7 III	14.99	−59.87	360^{+150}_{-80}	400	0.06	9 ± 2	<3.5	4×1200	1×1800
214080	6.8	B1/2 Ib	44.80	−56.92	$3700^{+\infty}_{-2800}$	3110	0.05	104 ± 3	213 ± 2	4×1200	1×1800
219639	6.6	B5 II/III	54.81	−65.63	610^{+1100}_{-240}	790	0.07	35 ± 3	68 ± 2	4×1200	1×1800 2×600
219833	7.2	A0 V	63.04	−63.68	520^{+480}_{-170}	200	0.03	8 ± 2	35 ± 3	3×1800	1×1800

dispersion (b) and column density (N). The best-fitting profiles, following convolution with the instrumental response function ($b_{\rm inst} \equiv 0.75/1.6651 = 0.45\,{\rm km\,s^{-1}}$), are shown superimposed on the data in Fig. 1, and the resulting line-profile parameters are listed in Table 2.

3 STELLAR DISTANCES AND RELATION TO THE 'CHIMNEY'

Clearly, the interpretation of the observed absorption-line profiles depends crucially on the stellar distances. Unfortunately, there is considerable uncertainty in the distances of several of these stars, as all but three lie well beyond the ∼500-pc limit of *Hipparcos* (at which distance the median precision of the measured parallaxes, $\Delta\pi \approx 1$ mas, amounts to about 50 per cent of the trigonometrical parallax, ESA 1997). For this reason, Table 1 also lists the photometrically derived distances, based on the published spectral types. Such distances are, of course, also notoriously unreliable, depending critically on the assumed spectral type (and especially the luminosity class). There is general agreement between the photometric and *Hipparcos* distances, given the errors, but in some cases the uncertainties are still so large that this comparison is of little help. For consistency within the present study, we have chosen tentatively to adopt the *Hipparcos* distances (rounded to the nearest 50 pc where appropriate) for the five stars where this is $\lesssim$600 pc. The adopted distances for all the stars are listed with the appropriate panels in Fig. 1. Only in the case of HD 208213 is this value very different from the photometric estimate. For the more distant star HD 214080 both the photometric and *Hipparcos* values suggest a distance of ∼3 kpc, and we will adopt that here.

In the case of HD 210191 (35 Aqr), there is a large disparity in the distance estimates and little independent evidence to decide between them. However, we may note that a distance as low as 350 pc, adopted by Lockman et al. (1986) on the basis of a B2.5 IV spectral type, is now excluded by the *Hipparcos* parallax. Matters are further complicated by an apparent ambiguity concerning the spectral type of this star. While that adopted here (B2 III) is derived from the generally reliable Michigan Catalogue (Houk & Smith-Moore 1988), and is similar to earlier determinations (e.g. B2 IV, Lesh 1968), the fact is that a spectral type as early as this makes it difficult to account for the observed strengths of the photospheric Ca K and Na D lines (Fig. 1).

While the strengths of the photospheric lines towards the other stars are generally consistent with the adopted spectral types, trial solar-metallicity LTE atmospheric modelling conducted using the spectrum synthesis code UCLSYN (Smith 1992) suggests an effective temperature of ∼11 000 K (i.e. a spectral type ∼B8/9) to account for the observed photospheric lines for HD 210191. Indeed, at B2 the photospheric Na D lines would not be expected to be detectable, and this region should instead be dominated by the C II 5889.78 Å–line (e.g. Crawford 1990), which is not observed. On the other hand, it is also true that a spectral type as late as B9 III results in a distance (only 190 pc) that is effectively excluded by the *Hipparcos* measurement. While the atmospheric modelling, particularly of the Ca line, provided some indication that log g might also be very low (∼2.5), indicative of supergiant status and a distance of ∼1600 pc (which *is* consistent with the *Hipparcos* measurement), it is clear that a much more careful analysis of the stellar spectrum will be needed to solve this particular puzzle. For the moment we tentatively adopt a distance of ∼1 kpc for HD 210191 as a compromise between the photometric and *Hipparcos* values, but note that this is very uncertain.

From the Galactic coordinates listed in Table 1 it can be seen that four of the seven stars (HD 208213, 209522, 210191 and 213728) lie within $\lesssim 10^\circ$ of a plane perpendicular to the Galactic plane and directed towards $l = 25^\circ$. Fig. 2(a) shows a slice through the 'Local Chimney' along this plane, produced using the method developed by Sfeir et al. (1999), and the projected locations of these four stars. It is clear that all four are located in the direction of the southern end of the Chimney, but at distances greater than the stars used to define it. Fig. 2(b) shows a similar diagram for the remaining three stars (HD 214080, 219639 and 219833), where the slice through the Chimney lies in the direction $l = 55^\circ$ (where, again, the stars lie within $\lesssim 10^\circ$ of this plane).

Fig. 3 shows the locations of the stars with respect to the low-velocity ($-50 \leqslant v_{\rm LSR} \leqslant +50$ km s^{-1}) H I distribution mapped by Hartmann & Burton (1997). From this we see that the total low-velocity H I column density towards the observed stars generally lies in the range $2 \pm 1 \times 10^{20}$ cm^{-2}. Clearly, it is of interest to determine

Downloaded from https://academic.oup.com/mnras/article-abstract/337/2/720/1026619 by Birkbeck College, University of London user on 12 August 2019

Table 2. Line profile parameters for the interstellar Ca K and Na D_2 lines towards the observed stars. The last column gives the Na I/Ca II column density ratio. Because two well-defined Na I components towards HD 219639 are observed to correspond to a broader, more poorly defined, Ca II feature, the later has been modelled as two componenst with velocities fixed to the Na I values; these are indicated by asterisks (but note that the −11.1 km s^{-1} Ca component is barely significant).

	Ca K			Na D_2			
Star (HD)	v_{LSR} (km s^{-1})	b (km s^{-1})	N ($\times 10^{10}$) (cm^{-2})	v_{LSR} (km s^{-1})	b (km s^{-1})	N ($\times 10^{10}$) (cm^{-2})	N(Na I)/N(Ca II)
208213	-19.3 ± 0.3	2.3 ± 0.3	25.5 ± 0.8	....	....	$\leqslant 3.0$	$\leqslant 0.12$
	-13.3 ± 3.0	3.2 ± 1.0	19.8 ± 2.9	....	....	$\leqslant 3.0$	$\leqslant 0.18$
	-8.6 ± 3.7	3.2 ± 1.0	16.9 ± 2.2	....	....	$\leqslant 3.0$	$\leqslant 0.20$
	-0.8 ± 0.4	2.7 ± 0.6	37.2 ± 1.2	-0.6 ± 0.5	1.6 ± 0.7	3.9 ± 3.2	0.11 ± 0.09
	$+2.9 \pm 0.6$	1.7 ± 0.8	11.7 ± 0.2	....	....	$\leqslant 3.0$	$\leqslant 0.26$
	$+7.2 \pm 1.2$	3.2 ± 1.5	9.6 ± 4.8	....	....	$\leqslant 3.0$	$\leqslant 0.63$
209522	-18.4 ± 0.1	2.1 ± 0.2	9.9 ± 0.7	-18.6 ± 0.3	1.3 ± 0.4	1.4 ± 0.8	0.14 ± 0.08
	-14.8 ± 0.3	0.8 ± 0.5	1.6 ± 0.3	....	....	$\leqslant 0.7$	$\leqslant 0.54$
	-11.2 ± 0.3	2.3 ± 0.6	8.2 ± 0.6	-12.2 ± 0.4	2.6 ± 0.6	3.4 ± 1.2	0.42 ± 0.15
	....	....	$\leqslant 1.4$	-9.2 ± 0.1	0.5 ± 0.2	3.1 ± 1.9	$\geqslant 0.86$
	-5.6 ± 0.6	3.7 ± 0.8	10.4 ± 0.6	-6.3 ± 0.1	0.6 ± 0.2	2.5 ± 1.3	0.24 ± 0.13
	$+2.5 \pm 0.1$	1.6 ± 0.1	33.2 ± 2.7	$+2.3 \pm 0.2$	2.7 ± 0.2	5.4 ± 0.1	0.16 ± 0.02
210191	-21.8 ± 0.1	1.6 ± 0.1	40.3 ± 2.7	-21.7 ± 0.1	1.16 ± 0.03	16.0 ± 2.2	0.40 ± 0.06
	-16.1 ± 0.1	1.6 ± 0.1	61.3 ± 3.7	-16.0 ± 0.1	1.11 ± 0.02	55.3 ± 1.9	0.90 ± 0.06
	-8.2 ± 0.1	2.5 ± 0.2	15.9 ± 0.1	....	....	$\leqslant 0.5$	$\leqslant 0.03$
	$+2.0 \pm 0.1$	0.9 ± 0.1	9.2 ± 1.8	$+2.0 \pm 0.1$	0.67 ± 0.07	8.0 ± 1.5	0.87 ± 0.24
	....	....	$\leqslant 1.8$	$+4.5 \pm 0.4$	1.4 ± 0.5	1.4 ± 0.5	$\geqslant 0.50$
	$+6.8 \pm 0.2$	2.2 ± 0.4	6.2 ± 0.2	....	....	$\leqslant 0.5$	$\leqslant 0.08$
213728	-12.8 ± 0.2	2.5 ± 0.3	7.3 ± 1.9	....	....	$\leqslant 0.8$	$\leqslant 0.15$
	$+14.0 \pm 0.3$	2.5 ± 0.5	5.3 ± 1.9	....	....	$\leqslant 0.8$	$\leqslant 0.24$
214080	-10.0 ± 0.3	2.9 ± 0.4	24.3 ± 5.6	-10.2 ± 0.1	0.44 ± 0.21	1.8 ± 0.1	0.07 ± 0.02
	-6.4 ± 0.1	1.0 ± 0.2	27.6 ± 8.5	-5.3 ± 0.1	1.28 ± 0.04	$490 \pm 59^{\dagger}$	17.8 ± 5.9
	-2.9 ± 0.1	2.6 ± 0.3	79.4 ± 14.0	-2.1 ± 0.1	1.90 ± 0.09	94.6 ± 7.2	1.19 ± 0.23
	$+2.1 \pm 0.1$	1.4 ± 0.2	32.0 ± 6.0	$+3.1 \pm 0.1$	0.84 ± 0.05	23.3 ± 2.5	0.73 ± 0.16
	$+5.9 \pm 0.4$	1.4 ± 0.6	4.4 ± 3.1	$+5.8 \pm 0.2$	1.74 ± 0.21	10.0 ± 2.9	2.27 ± 1.73
219639	-11.1^{*}	1.8 ± 0.8	3.9 ± 3.8	-11.1 ± 0.2	1.2 ± 0.3	1.8 ± 0.8	0.46 ± 0.49
	-8.1^{*}	2.5 ± 0.8	8.6 ± 4.8	-8.1 ± 0.1	1.3 ± 0.1	9.3 ± 1.0	1.08 ± 0.61
	-3.0 ± 0.1	0.9 ± 0.1	24.1 ± 5.8	-3.2 ± 0.1	1.57 ± 0.03	34.3 ± 1.3	1.42 ± 0.35
	-0.4 ± 0.2	1.1 ± 0.3	9.8 ± 3.9	$+0.8 \pm 0.1$	0.85 ± 0.14	2.1 ± 0.7	0.21 ± 0.11
219833	-7.5 ± 0.2	1.1 ± 0.3	7.9 ± 1.6	-7.2 ± 0.1	1.2 ± 0.2	8.7 ± 2.5	1.10 ± 0.39
	-3.0 ± 0.2	1.7 ± 0.4	9.6 ± 1.9	-3.6 ± 0.4	2.5 ± 0.5	10.0 ± 2.7	1.04 ± 0.35

*Ca II velocities fixed at Na I values; see the table caption.

†Note that this component is fully saturated in Na D_2 and N is constrained by the weaker D_1 line; however, as D_1 itself reaches a residual intensity of just 1 per cent, the resulting N is uncertain and should probably be viewed as a lower limit.

whether the present observations of absorption lines are able to place limits on the distance to this H I. Na I is often used as a tracer for hydrogen in the diffuse interstellar medium, and Ferlet, Vidal-Madjar & Gry's (1985) relationship implies that (with the notable exception of HD 214080) much of the H I mapped at 21 cm lies beyond the stars. Unfortunately, Ferlet et al.'s relation actually displays considerable scatter, and suffers from order-of-magnitude uncertainties at low [N(Na I) $\lesssim 10^{11}$ cm^{-2}] column densities (e.g. Welty et al. 1994; Wakker & Mathis 2000). However, even allowing for this uncertainty, it does appear that at least in the cases of HD 208213 and 213728 [for which the Ferlet et al. relation predicts N(H I) $\sim 8 \times 10^{18}$ and $\lesssim 4 \times 10^{18}$ cm^{-2}, respectively] the bulk of the H I lies in the background (i.e. at distances $\gtrsim$500 pc). This is rather further than expected from the notional extent of the Lockman layer, but quite consistent with the greater scaleheights found for Ca II and Ti II by Albert et al. (1993). Finally, we note that while the one star with a significantly greater Na I (and thus inferred H) column density, HD 214080, is also the most distant, Fig. 1 indicates that most of this is contributed by a single, strong velocity component at $v_{LSR} = -5.3$ km s^{-1}, presumably a result of a dense interstellar cloud relatively close to the Sun (and perhaps associated with the Chimney boundary; cf. Fig. 2b).

4 DISCUSSION

4.1 The velocity structure

Much of the interpretation of the present data hinges on the radial velocities of the observed interstellar absorption components. Thus, after a brief discussion of the stellar radial velocities and possible *circumstellar* absorption, we will discuss how the observed velocities relate to those expected from Galactic rotation and

Downloaded from https://academic.oup.com/mnras/article-abstract/337/2/720/1026619 by Birkbeck College, University of London user on 12 August 2019

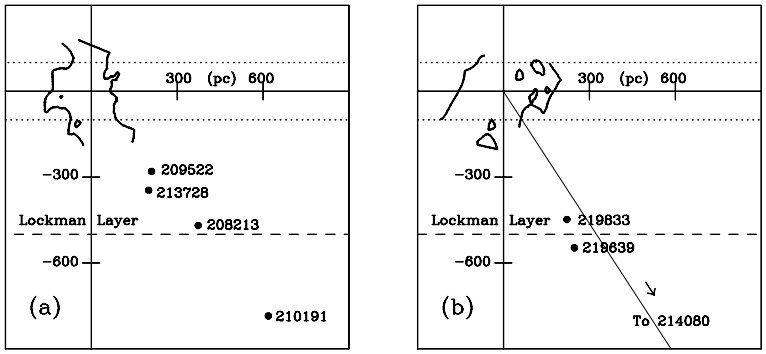

Figure 2. Locations of the observed stars relative to the Local Chimney. As discussed in the text, the plot shows two slices perpendicular to the Galactic plane: (a) towards $l = 25^\circ$ and (b) towards $l = 55^\circ$. The Sun is located at the origin, and a scale in parsecs is provided. The irregular solid lines mark the boundary of the 'Local Chimney' as defined by Sfeir [1999, i.e. the boundary at which the total interstellar Na I D_2 equivalent width reaches 50 mÅ, or $N(\mathrm{H\,I}) \sim 5 \times 10^{19}$ cm^{-2}], and are based on data for 126 and 107 stars for (a) and (b), respectively. The dotted and dashed lines indicate the scaleheights of the cool H I and warm Lockman layers, respectively, and it is apparent that the total length of the 'Chimney' is well matched to the former, as would be expected. The sloping line in (b) indicates the direction to the very distant HD 214080.

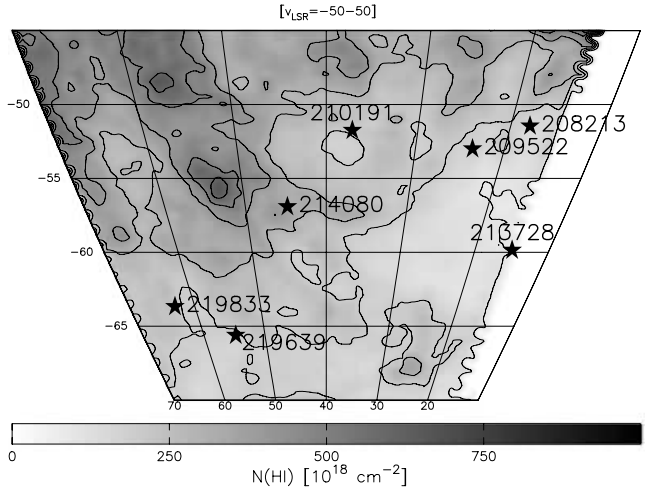

Figure 3. Map showing the locations of the observed stars with respect to the low-velocity ($-50 < v_{\mathrm{LSR}} < +50$ km s^{-1}) H I column density distribution mapped by Hartmann and Burton (1997); contours are set at 1, 2, 3, 4, 5 and 6×10^{20} cm^{-2}.

other phenomena known to affect the kinematics of the interstellar medium.

4.1.1 Stellar velocities and possible circumstellar absorption

Table 3 lists the LSR radial velocities of the stars, where published values are available from SIMBAD, and/or where they are obtainable from the photospheric Ca K and Na D lines observed here. Before proceeding, a brief comment on the apparent discrepancies between the stellar Ca and Na velocities for HD 210191 and 213728 is required. In the former case, the discrepancy amounts to only 4 km s^{-1} and, given that the overall Ca K profile is heavily affected by complex interstellar structure (Fig. 1) the Na D value may be the more reliable one. As one of the two Ca spectra was obtained on the same night as the single Na spectrum, and only 3 h earlier, a variable stellar radial velocity is unlikely to be a plausible explanation. However, the fact that both of these velocities are significantly more negative than the published value of -1.8 km s^{-1} may nevertheless indicate that HD 210191 is a possible long-period spectroscopic binary (although no such companion ever seems to have been identified; e.g. Abt & Cardona 1984). In the case of HD 213728, the tentative identification of the broad, shallow feature at $+3.5$ km s^{-1} with the photospheric Na D_2 line is rendered problematical by the absence of a correspondingly broad D_1 line; clearly further work on the stellar spectrum of this star is required before making too much of the apparent velocity discrepancy noted in Table 3.

As discussed at some length in an earlier paper (Crawford 2001a, Section 3.2), narrow absorption lines occurring close to the radial velocity of the star may arise in the circumstellar environment. This is particularly true of Ca II lines towards A-type stars (e.g. Holweger, Hempel & Kamp 1999), when it can be very difficult to distinguish unambiguously between interstellar and circumstellar contributions. However, the only A-type star in the present sample is HD 219833, and there are no components centred at the stellar radial velocity in this case.

The clearest case for possible circumstellar absorption in the present data set is the -8.2 km s^{-1} Ca II component in the spectrum of HD 210191. Not only does this occur exactly at the centre of the broad stellar line, but the lack of any corresponding feature in Na I results in an extreme Na I/Ca II upper limit (<0.03; Table 2) which is sometimes also taken to be diagnostic of circumstellar absorption (for example, the well-known circumstellar component in the spectrum of β Pictoris has a similarly low value; Hobbs et al. 1985). Looking at the spectrum, it is even conceivable that what appears to be a discrete line at -8.2 km s^{-1} could actually be the narrow core of a non-Gaussian photospheric line (although the photospheric line modelling discussed above would not lead us to expect such a profile). Another slightly 'suspicious' Ca II component, given its relative breadth, lack of corresponding Na, and location with respect to the stellar line, is that at -12.8 km s^{-1} towards HD 213728. However, in the absence of any additional information with which to discriminate between circumstellar and interstellar lines we will tentatively retain these components in the interstellar analysis.

4.1.2 Galactic rotation

The velocity range that we expect to be occupied by interstellar material corotating with the Galaxy may be calculated from the Galactic coordinates of each line of sight and a rotation curve for the Milky Way. Adopting the rotation curve of Fich, Blitz & Stark (1989), we

Downloaded from https://academic.oup.com/mnras/article-abstract/337/2/720/1026619 by Birkbeck College, University of London user on 12 August 2019

Table 3. The LSR radial velocity ranges expected to arise from Galactic rotation [$v_{\rm LSR}$ (Galaxy)] and, where appropriate, the near (−) and far (+) sides of the expanding Loop II bubble [$v_{\rm LSR}$ (Loop II)] towards the observed stars. The next two columns give the stellar radial velocities, where $v^*_{\rm LSR}$(SIMBAD) are the published values on the SIMBAD data base (where available), and $v^*_{\rm LSR}$ (Here) are the values obtained here from the observed stellar Ca K and Na D lines. The number in the last column ($\Delta v^{\rm LSR}_{\rm helio}$) should be *added* to the LSR velocities to give the heliocentric values.

Star (HD)	$v_{\rm LSR}$ (Galaxy) (km s^{-1})	$v_{\rm LSR}$ (Loop II) (km s^{-1})	$v^*_{\rm LSR}$ (SIMBAD) (km s^{-1})	$v^*_{\rm LSR}$ (Here) (km s^{-1})	$\Delta v^{\rm LSR}_{\rm helio}$ (km s^{-1})
208213	−0.4 to +1.4	....	−64.8	....	−2.2
209522	−0.5 to +0.5	....	....	....	−2.3
210191	−0.8 to +3.8	±6.6	−1.8	−8.1 (Ca) −12.0 (Na)	−3.4
213728	−0.3 to +0.4	....	....	−20.7 (Ca) +3.5 (Na)?	+0.1
214080	−0.8 to +6.3	±9.1	+2.2	+8.4 (Ca)	−2.2
219639	−0.7 to +0.4	±10.1	....	−13.4 (Ca)	+0.2
219833	−0.8 to +5.9	±11.8	....	+5.7 (Ca)	−0.3

obtain the projected line-of-sight velocities given in Table 3, and these are indicated by vertical dashed lines in Fig. 1. For all the stars discussed here, even the very distant HD 214080, the radial velocity resulting from Galactic rotation increases almost linearly with distance. Thus, of the velocity range delineated in Fig. 1, the lower boundary corresponds to local material, essentially at rest with respect to the LSR. The upper limits are then the velocities predicted at the adopted stellar distances. We note that the velocity range expected to arise from Galactic rotation is much more restricted at these high Galactic latitudes than it would be in the plane, owing to the strong latitude dependence (e.g. Cohen 1975).

It is apparent from Fig. 1 that most of these stars do have absorption components within, or at least close to (i.e. within ∼5 km s^{-1}), the velocity range expected from Galactic rotation. However, it is notable that they all also exhibit absorption components outside this range, and in all cases except the +14 km s^{-1} component towards HD 213728 these occur at more *negative* velocities. It is important to realize that, for stars in this Galactic longitude range and at these distances, significant negative LSR velocities are contrary to the sense of Galactic rotation, and so must arise from some other cause. This tendency for high Galactic latitude absorption to exhibit peculiar velocities with respect to a halo corotating with the disc has, in fact, already been noted in several earlier studies (e.g. Albert et al. 1993, and references therein). Note, that while Albert et al. identified examples of *positive* peculiar velocities towards two of the present stars (HDs 210191 and 214080), the higher resolution employed here enables us to identify these with the red wings of the photospheric lines (compare the relevant panels of our Fig. 1 with their fig. 2). Thus, in the present sample all the peculiar interstellar velocities (with the single exception of the weak +14 km s^{-1} Ca II component towards HD 213728) are negative, and we now turn to a discussion of possible explanations for them.

4.1.3 *Interstellar bubbles*

A common origin of high-velocity, especially high negative velocity, interstellar absorption components are the expanding shells and bubbles associated with OB associations [first discussed by Münch (1957), and subsequently studied by many other authors; see Crawford, Barlow & Blades (1989) for a brief summary]. Although these structures are generally located close to the Galactic plane, this being the location of the OB associations responsible for them, it is possible in principle for even quite high-latitude lines of sight to penetrate relatively nearby shells that subtend large angular sizes on the sky. This possibility is graphically illustrated by Gahm (1994) who has compiled a list of all the known interstellar bubbles within 1 kpc, several of which extend to $|b| \gtrsim 60^\circ$.

However, it turns out that the only known interstellar bubble in the foreground to the stars observed here is the very large non-thermal radio continuum structure known as Loop II (otherwise known as the Cetus Arc; e.g. Large, Quigley & Haslam 1962; Berkhuijsen 1973; Vallée 1994). Indeed, we find that these seven stars actually straddle the Loop II boundary. Given the well-determined Loop II centre ($l = 100^\circ$, $b = -32.5^\circ$), Fig. 4 shows the extent of this feature on the sky, for both a radius of 45°, which is the radius of peak emission, and the larger 'half-power' radius of 53° obtained by Berkhuijsen (1973), which we take to be a conservative upper limit for its maximum extent. We see that HD 208213, 209522 and 213728 certainly

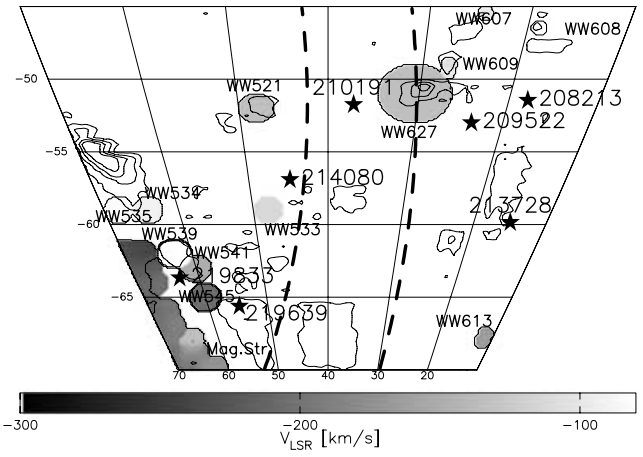

Figure 4. Map showing the distribution of the observed stars with respect to the Loop II shell (Berkhuijsen 1973) and known HVC and IVC complexes (Bajaja et al. 1985; Hulsbosch & Wakker 1988; Morras et al. 2000). The inner (leftmost) dashed line marks the canonical, 45°, radius of peak emission for Loop II, while the outer dashed line marks the 53° 'half-power' radius obtained by Berkhuijsen (1973). Catalogued HVCs (grey-scaled polygons) are marked with their identification numbers from Wakker & van Woerden (1991). The dense clustering of very high-velocity HVCs to the lower left of the figure is part of the Magellanic Stream and lies well in the background (∼50 kpc; e.g. Gardiner & Noguchi 1996). The irregular, unshaded, contours mark the known locations of IVCs ($-150 < v_{\rm LSR} < -50$ km s^{-1}), most having column densities N(H I) $\approx 2 \times 10^{19}$ cm^{-2}.

Downloaded from https://academic.oup.com/mnras/article-abstract/337/2/720/1026619 by Birkbeck College, University of London user on 12 August 2019

lie outside Loop II on the sky, and HD 214080, 219639, 219833 certainly lie within it; HD 210191 lies close to the boundary, but lies just within it if we adopt the larger radius given by Berkhuijsen (1973). Following Gahm (1994) and adopting this larger size, the projected LSR radial velocities for the near and far sides of Loop II for the four stars found within it are given in Table 3, where we have adopted an expansion velocity of 19 km s^{-1} (Vallée 1994). It is immediately apparent that while Loop II might, in principle, account for low negative velocity ($v_{\rm LSR} \approx -10$ km s^{-1}) absorption towards HD 214080, 219639 and 219833, it cannot plausibly account for the highest blueshifted velocities observed here ($v_{\rm LSR} \lesssim -15$ km s^{-1}). Given the high Galactic latitudes, it is unlikely that more distant, as yet unrecognized, OB association bubbles exist in the foreground to these stars.

4.1.4 High-velocity clouds

In principle, highly blueshifted (or redshifted) interstellar absorption lines at high Galactic latitudes could be associated with the high- and intermediate-velocity clouds (HVCs and IVCs, respectively) detected in 21-cm H I surveys (e.g. Wakker & van Woerden 1997; Wakker 2001 and references therein). Although the distances that have been estimated to-date for a relatively small number of HVCs and IVCs would lead us to expect them to lie well beyond the stars observed here, it is nevertheless of interest to determine whether the current observations can yield any useful information concerning such structures in this direction.

The total velocity coverage of the present spectra, of which only a small part is shown in Fig. 1, was -350 to $+200$ km s^{-1} for Ca K, and -450 to $+100$ km s^{-1} for Na D$_1$ (Na D$_2$ extending to only -130 km s^{-1} owing to the placement of the doublet on the detector). No velocity components were detected in either species within these velocity ranges, other than the low-velocity components shown in Fig. 2. Depending only slightly on the signal-to-noise ratios of the individual spectra, these non-detections imply Na I column density limits of $\lesssim 10^{10}$ cm^{-2} for any HV gas that may be present. The corresponding H I limits, based on the relationship of Ferlet et al. (1985) are then $\lesssim 10^{18}$ cm^{-2} (but note the order-of-magnitude uncertainty on this relationship discussed in Section 3).

Fig. 4 shows the distribution of HVC and IVC structures in the direction of the stars observed here (Bajaja et al. 1985; Hulsbosch & Wakker 1988; Morras, Bajaja & Pöppel 2000). Unfortunately, there are only a few coincidences in position between the stars and the HV/IV clouds, limiting the conclusions that can be drawn. HD 219639 does project on to an IVC and the absence of corresponding Na I absorption (with the limits given in Table 3) may imply a distance $\gtrsim$600 pc for this cloud. However, as discussed by Wakker (2001), it is important to realize that this conclusion depends on the assumption of detectable column densities being present within the IVC, which, for a given line of sight, may also depend on the degree of clumping in the cloud (e.g. Shaw et al. 1996). In this case, if the Na I and Ca II abundances were at the low end of values typically found for IVCs, or if the sightline passed between clumps, then this one might not have been detected here even if it were closer than the star. Similarly, the lack of IV absorption towards HD 213728 may imply a distance $\gtrsim$400 pc for the IVC close to its position (although in this case the positional coincidence is not exact).

4.2 Evidence for infall?

Summarizing the above, it seems clear that neither the foreground Loop II shell, or the background HVC/IVC complexes, can account for the moderately negative velocity absorption ($-25 \lesssim v_{\rm LSR} \lesssim -10$ km s^{-1}) observed towards HDs 208213, 209522 and 210191. While in no sense extreme by interstellar standards, the fact that these velocities are contrary to the sense of Galactic disc rotation implies that they represent a different kinematical component, presumably in the lower halo, or material that is falling towards the Galactic plane from higher z.

The three stars that exhibit these components all lie fairly close together on the sky (cf. Figs 4 and 2a), and a broadly co-spatial origin at a distance $\lesssim$350 pc (the distance to the nearest star of the three) may be implied. On the other hand, although the uncertainties in the stellar distances make it hard to be definitive (Table 1), it seems that while the gross velocity structure is similar, the *strengths* of the lines in this velocity range increase with distance. Moreover, strong Na I lines are present in this velocity range towards HD 210191 (at $\sim$1 kpc) that are absent for the nearer stars. These considerations actually argue against a purely local ($\lesssim$350 pc) location for this material, and instead suggest that the lower halo gas in this direction occupies a common velocity range ($-25 \lesssim v_{\rm LSR} \lesssim -10$ km s^{-1}). In this interpretation weak components, similar to those towards the nearer stars, would also be present towards HD 210191, but masked by stronger absorption arising from more distant gas sharing the same infall velocity.

These three stars lie in areas 22 (HD 210191) and 23 (HDs 208213 and 209522) defined by Albert et al. (1993) in their study of halo structure. Albert et al. observed several other stars in each of these areas (cf. their table 1), which may in principle be used to constrain the closest distance to which this blueshifted material approaches the Galactic plane. It turns out that no absorption components in the velocity range of interest here were detected towards any of the other (five) stars in these areas excluding the present three. With the exception of the very distant ($\sim$4 kpc) HD 206144 (where the relevant velocity range is obscured by blending with a stronger low-velocity component), the *Hipparcos* parallaxes (ESA 1997) all yield distances of approximately 200 pc. Thus the non-detection of anomalous blueshifted components towards these stars by Albert et al. (1993) may imply a lower limit of 200 pc for the closest infalling material in this direction (although it would of course be desirable to repeat the study of Albert et al. with the same spectral resolution as employed here to confirm this conclusion).

Fig. 4 shows that HDs 208213, 209522 and especially HD 210191, all lie close to high-velocity gas associated with WW627. Although the velocities are lower than the corresponding H I emission (~ -135 km s^{-1}), it is interesting to note that Kalberla et al. (1997) have recently drawn attention to what they call 'velocity bridges' of H I, which seem to connect a number of HVCs with low-velocity material. Further studies may therefore be warranted to determine whether the 'common infall' velocities observed here in the general direction of WW627 represent a detection of the same phenomenon in optical absorption lines. Clearly, should such a physical connection be demonstrated, it would imply an interaction between HVCs and the lower halo, with possibly far-reaching implications for our understanding of halo structure. Note that some limits may be placed on the spatial extent of this infall region by noting the absence of absorption in this velocity range towards HD 213 728 and 214080. Clearly, the observation of many more stars in this area of sky, and at a range of distances, will be required to confirm the existence of a discrete region displaying common infall velocities, and to check for any connection with the (presumably background) HVC WW627.

Downloaded from https://academic.oup.com/mnras/article-abstract/337/2/720/1026619 by Birkbeck College, University of London user on 12 August 2019

4.3 The *b*-values

The primary line-broadening mechanisms in the neutral interstellar medium are thermal Doppler broadening and broadening caused by bulk motions of the gas ('turbulence'). These combine to produce an observed velocity dispersion, b, as follows:

$$b = \sqrt{\frac{2kT_{\rm k}}{m_A} + 2v_{\rm t}^2}, \quad (1)$$

where $T_{\rm k}$ is the kinetic temperature, $v_{\rm t}$ is the line-of-sight turbulent velocity, k is Boltzmann's constant and m_A is the mass of the element (atomic mass A) under observation. This equation can be used to place constraints on the physical conditions of the absorbing medium. In particular, by setting $v_{\rm t} = 0$ it is possible to use an observed b-value to obtain a rigorous upper limit to the kinetic temperature, $T_{\rm k}^{\rm ul}$.

One of the primary aims of the present project was to exploit the extremely high resolving power of the UHRF to search for evidence of broader than usual interstellar lines towards these high-latitude stars. This is of particular interest for the more distant objects, where the lines of sight should probe the warm/hot 'Lockman' and 'Reynolds' layers, and where warmer and/or more turbulent gas might be expected. Indeed, some previous work (e.g. Danly 1989) has claimed the detection of very broad ($b \approx 100$ km s^{-1}) absorption lines towards halo stars, but it now appears more likely that these extreme widths result from the failure to resolve all the velocity components in the line of sight. For example, on the basis of *IUE* data, Danly (1989) found interstellar absorption with a FWHM of $\sim$50 km s^{-1} (centred at $v_{\rm LSR} \sim 0$ km s^{-1}) towards HD 214080, but the present observations (Fig. 1, Table 2) reveal no less than five discrete absorption components in this velocity range (note that the difficulty of resolving this structure in the UV results not only from the lower resolution employed, but also from the intrinsically much stronger lines).

Fig. 5 shows the b-values obtained here plotted as a function of LSR velocity, and it is clear that, while there is a certain amount of scatter, the values for individual clouds are all quite modest. On the other hand, it is true that the median b-values (2.10 km s^{-1} for Ca II and 1.28 km s^{-1} for Na I) are somewhat larger than the values typically found for comparably well-resolved clouds closer to the Galactic plane. For example, the extensive Ca II survey of Welty, Morton & Hobbs (1996) found a median Ca II b-value of 1.31 km s^{-1}, while the companion Na I survey of Welty et al. (1994) found a median Na I b-value of 0.73 km s^{-1}. Thus, there is some evidence that, taken as a whole, the high-latitude clouds studied here are somewhat hotter and/or more turbulent than those found closer to the Galactic plane.

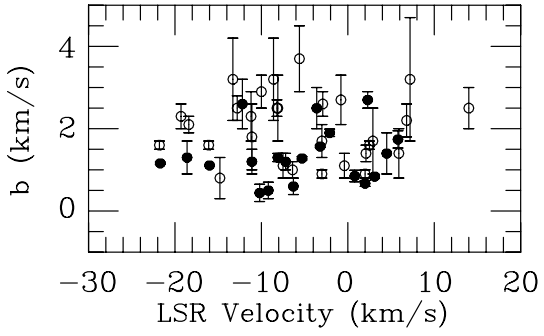

Figure 5. The velocity dispersions (b-values) of the identified velocity components, plotted as a function of LSR velocity. Open circles represent Ca II, while solid circles represent Na I. Note that Ca II generally has the larger b-values, despite being the heavier ion, and that there is no dependence of b-values on velocity.

That being said, however, it is also clear that the observed b-values provide little evidence for gas as warm as usually envisaged for the Lockman layer. In the case of Na I, a temperature of 6000 K would (in the absence of turbulence) result in a b-value of 2.1 km s^{-1}, and Table 2 reveals that only four components out of 21 (19 per cent) have values as large as this within the quoted errors. The median b-value (1.28 km s^{-1}) corresponds to a rigorous temperature upper limit of $T_{\rm k}^{\rm ul} = 2300$ K, and for the many components with Na I b-values clustering around 1 km s^{-1} (Fig. 5) $T_{\rm k}^{\rm ul} = 1400$ K (and any non-zero turbulence would reduce the actual temperature further). Thus there seems little doubt that even well out into the region supposedly occupied by the Lockman layer, much of the gas actually exists in discrete clouds at much lower temperatures.

On the other hand, it is also clear from Fig. 5 that the Ca II b-values would permit higher temperatures, and that the tendency (well-documented at lower latitudes) for b(Ca) to exceed b(Na), also holds for these high-latitude clouds. It follows from equation (1) that absorption lines arising from co-spatial Ca and Na ions must be characterized by $0.76 < b({\rm Ca})/b({\rm Na}) < 1.00$ (where the limits correspond to pure thermal and pure turbulent broadening, respectively). Thus, while the generally excellent velocity agreement between Ca II and Na I (Table 1) certainly implies that the two species are physically associated, there can be no doubt that the Ca II ions are located in a warmer and/or more turbulent medium than those of Na I, presumably in the outer, less well shielded regions of the absorbing structures.

4.4 Na I/Ca II ratios

The Na I/Ca II column density ratio is well known as a diagnostic of the physical conditions prevailing in diffuse interstellar clouds, mostly because Ca is much more susceptible than Na to the balance between adsorption on, and desorption from, interstellar grains (e.g. Jura 1976; Barlow 1978; Phillips, Pettini & Gondhalekar 1984; Cardelli, Federman & Smith 1991). Specifically, cold ($T_{\rm k} \sim 30$ K), dense ($n_{\rm H} \gtrsim 10^3$ cm^{-3}) diffuse molecular clouds, where most of the gas-phase Ca is depleted on to grains, generally exhibit Na I/Ca II $\gtrsim 100$, whereas values two or more orders of magnitude lower are expected in warmer ($T_{\rm k} \sim 10^3$ K), lower-density ($n_{\rm H} \approx 10$ cm^{-3}) material where much of the available Ca remains in the gas phase (e.g. Hobbs 1976; Centurion & Vladilo 1991; Crawford 1992; Bertin et al. 1993). It must be understood, however, that even where the same velocity component is identified in both species, the fact that Na I and Ca II do not dominate in the same *regions* of a given cloud means that physical characteristics deduced from the ratio can at best only be a crude average for the cloud as a whole.

The Na I/Ca II ratios for the absorption components identified here are plotted in Fig. 6, and two things are immediately apparent. First, that there is no clear dependence of Na I/Ca II on velocity, and secondly that the observed ratios are uniformly very low (with only one exception, all being $\lesssim$1.0, with several $\lesssim$0.1). These low values are in fact quite typical of values found within the local interstellar medium (LISM; e.g. Bertin et al. 1993), which may suggest similar patterns of depletion throughout the Local Interstellar Chimney, and perhaps far out into the lower halo. On the other hand, it is also possible, in principle, that the low Na I/Ca II are only coincidentally LISM-like, and actually arise from the shock-wave disruption of interstellar grains [for example, some of the lower values found here are similar to those observed in Vela supernova remnant by Hobbs,

Downloaded from https://academic.oup.com/mnras/article-abstract/337/2/720/1026619 by Birkbeck College, University of London user on 12 August 2019

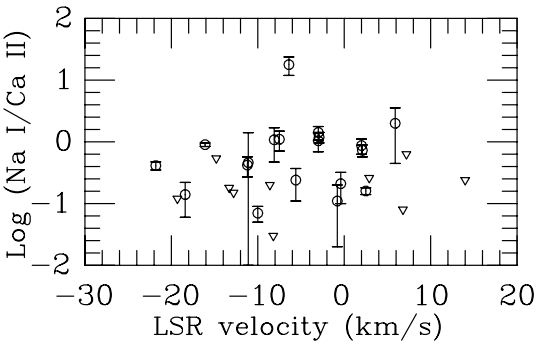

Figure 6. The Na I/Ca II column density ratios of the observed velocity components, plotted as a function of LSR velocity. Downward-pointing triangles indicate upper limits.

Wallerstein & Hu (1982)], or by anomalous ionization conditions far from the Galactic plane.

However, the lack of dependence of Na I/Ca II on velocity argues against grain destruction by interstellar shocks. At first sight the lack of a velocity dependence is surprising, given that much earlier work (Routly & Spitzer 1952; Siluk & Silk 1974; see also Crawford et al. 1989 and references therein) has shown that there is generally a fairly strong anticorrelation between the two, usually attributed to the removal of adsorbed Ca atoms from grain surfaces by shocks in the higher-velocity gas. However, as pointed out by Crawford et al. (1989), this apparent velocity dependence may equally be explained by the fact that dense, slowly moving, high-Na I/Ca II ratio material will mask any lower ratio material arising in warmer and/or less dense clouds that happen to occupy the same velocity range.

A prediction of this idea is that sightlines free from dense clouds should exhibit low-Na I/Ca II ratio material at low velocities as well as high. This has been borne out by several more recent studies (e.g. Vallerga et al. 1993; especially their fig. 6), and is well illustrated by the present data (Fig. 6). With the exception of the −6.4 km s^{-1} component towards HD 214080, dense foreground clouds are absent here (owing to the sightlines being through the Chimney) and Na I/Ca II $\lesssim 1.0$ material is indeed found to extend across the whole velocity range. The lack of a Routly–Spitzer effect in these data indicates that the Na I/Ca II ratios are not a result of enhanced shock processing in high-velocity gas, which is the usual interpretation, but have some other cause. The most likely explanation is that the densities are sufficiently low that Ca depletions remain modest over the cloud lifetime; for example, the Ca depletion time-scale is $\sim 2.2 \times 10^7$ yr for $n_{\rm H} \sim 10$ cm^{-3} and $T_K \sim 5000$ K (cf. equation (3) of Crawford 2001b).

An alternative explanation for low Na I/Ca II ratios was proposed by Pottasch (1972), who argued that at temperatures $\gtrsim$7000 K collisional ionization of Na I would be expected to lead to a sharp reduction in this quantity. Given that many of the components observed here arise far from the plane, within the region supposedly occupied by the high-temperature Lockman and Reynolds layers, it is especially important to examine this possibility here. Although White (1974) long ago raised the objection that Pottasch's interpretation would clash with the observed abundances of *neutral* calcium (Ca I), the advent of ultrahigh-resolution spectroscopy provides us with an unambiguous test through the measured linewidths.

In the present case, we find no less than six separate absorption components with $b_{\rm Ca} \lesssim 1.4$ km s^{-1} ($T_{\rm k}^{\rm ul} \lesssim 5000$ K, such that collisional ionization of Na I will be negligible; Pottasch 1972), *and* Na I/Ca II $\lesssim 1.0$ (Table 2). The temperature upper limits imposed by the Na *b*-values are even tighter. Perhaps the clearest example is provided by the well-defined +2.0 km s^{-1} component towards HD 210191, for which b(Ca) $= 0.9 \pm 0.1$ km s^{-1} and b(Na) $= 0.67 \pm 0.07$ km s^{-1}. These correspond to rigorous temperature upper limits of $T_{\rm k}^{\rm ul}$(Ca) $= 1950 \pm 430$ K and $T_{\rm k}^{\rm ul}$(Na) $= 620 \pm 130$ K, and yet Na I/Ca II $= 0.87 \pm 0.24$. Thus, the Pottasch effect can be securely excluded for this component and others like it.

5 CONCLUSIONS

The main conclusions of the present work are as follows.

(i) We have obtained high-resolution observations of interstellar Ca II and Na I lines towards seven stars in the direction of the southern opening of the recently identified Local Interstellar Chimney (Welsh et al. 1999). These lines of sight probe the lower Galactic halo ($0.3 \lesssim |z| \lesssim 2.5$ kpc), without the complication of sampling dense foreground interstellar material.

(ii) We have detected 31 discrete absorption components towards these stars (Table 2), many of them undetected in previous lower-resolution studies. We argue that some of the very broad absorption lines previously reported for halo lines of sight have resulted from the failure to resolve this complicated velocity structure.

(iii) In addition to components with velocities close to those expected from Galactic rotation, all of these stars also exhibit components with negative LSR velocities, which is contrary to the sense of Galactic rotation for the directions observed. While the low negative velocity ($v_{\rm LSR} \approx -10$ km s^{-1}) absorption towards three stars (HDs 214080, 219639 and 219833) might plausibly result from the sightlines intercepting the near side of the expanding Loop II bubble (Section 4.1.3), this explanation cannot account for the higher blueshifted ($v_{\rm LSR} \lesssim -15$ km s^{-1}) velocities found towards three other stars (HDs 208213, 209522 and 210191). These latter three stars lie relatively close together on the sky (Fig. 4), and may sample a restricted volume of the inner halo subject to common infall velocities over a large distance range (∼350–1000 pc). Further observations of many more stars, at a range of distances, are needed to confirm this interpretation, and any possible connection with the (presumably background) HVC WW627 (Fig. 4).

(iv) The observed *b*-values are generally very small (Table 2), and although the median values are slightly larger than those typically found in the Galactic disc (implying somewhat warmer and/or more turbulent clouds at high $|z|$; Section 4.3), the Na I *b*-values are inconsistent with temperatures as high (∼6000 K) as generally assumed for the Lockman layer. While we should bear in mind the possibility that the lower halo in the vicinity of the Chimney may be atypical, we find no evidence for a continuous medium with this temperature corotating with the Galactic disc and having a scaleheight of ∼500 pc, as originally envisaged by Lockman et al. (1986).

(v) The Na I/Ca II ratios of these components are all very low ($\lesssim$1.0, with several <0.1; Fig. 6), and show no dependence on cloud velocity. Although it is tempting to attribute these low values to the enhanced destruction of grains far from the plane, they are in fact quite typical of values found in the local interstellar medium (i.e. within 50 pc of the Sun; e.g. Bertin et al. 1993). The absence of high Na I/Ca II material at low LSR velocities (as expected from the Routly–Spitzer effect) is (with the single exception of one velocity component towards HD 214080) solely a result of the absence of dense foreground clouds within the Chimney.

(vi) Taking all of this into account, the picture that emerges is of a scattered, generally infalling, population of discrete diffuse

Downloaded from https://academic.oup.com/mnras/article-abstract/337/2/720/1026619 by Birkbeck College, University of London user on 12 August 2019

clouds, not unlike those commonly found in the local interstellar medium (i.e. with relatively cool interiors surrounded by warmer and/or more turbulent haloes), which extends for many hundreds of parsecs above the plane. However, for the bias towards infall (already noted by many previous authors), this would support the modified view of the H I distribution advanced by Lockman & Gehman (1991), where the extent of the neutral medium is maintained by the motions of individual clouds within the Galactic gravitational potential. However, as already noted by Lockman & Gehman, the apparent lack of *redshifted* halo components strongly implies that the *outflowing* gas does not exist in the same form. Overall, then, our observations seem most consistent with the 'Galactic fountain' model of Shapiro & Field (1976), where hot, fully ionized, gas rises into the halo as a fountain, but descends in the form of neutral clouds such as those observed here.

ACKNOWLEDGMENTS

We thank PATT for the award of telescope time, and Elly Berkhuijsen for helpful correspondence on the structure of Loop II. IAC and RJP thank PPARC for the awards of an Advanced Fellowship and a Research Studentship, respectively.

REFERENCES

Abt H.A., Cardona O., 1984, ApJ, 285, 190
Albert C.E., Blades J.C., Morton D.C., Lockman F.J., Proulx M., Ferrarese L., 1993, ApJS, 88, 81
Barlow M.J., 1978, MNRAS, 183, 417
Bajaja E. et al., 1985, ApJS, 58, 143
Berkhuijsen E.M., 1973, A&A, 24, 143
Bertin P., Lallement R., Ferlet R., Vidal-Madjar A., 1993, A&A, 278, 549
Bregman J., Harrington J., 1986, ApJ, 309, 833
Cardelli J.A., Federman S.R., Smith V.V., 1991, ApJ, 381, L17
Centurion M., Vladilo G., 1991, ApJ, 372, 494
Cohen J.G., 1975, ApJ, 197, 117
Cox D.P., Reynolds R.J., 1987, ARA&A, 25, 303
Crawford I.A., 1990, Observatory, 110, 145
Crawford I.A., 1992, MNRAS, 259, 47
Crawford I.A., 2001a, MNRAS, 327, 841
Crawford I.A., 2001b, MNRAS, 328, 1115
Crawford I.A., Barlow M.J., Blades J.C., 1989, ApJ, 336, 212
Crawford I.A., Craig N., Welsh B.Y., 1997, A&A, 317, 889
Crawford I.A., Lallement R., Welsh B.Y., 1998, MNRAS, 300, 1181
Danly L., 1989, ApJ, 342, 785
de Boer K.S., 1998, LNP, 506, 433
Diego F., 1993, Appl. Opt., 32, 6284
Diego F. et al., 1995, MNRAS, 272, 323
ESA, 1997, The *Hipparcos* and *Tycho* Catalogues, ESA SP-1200
Ferlet R., Vidal-Madjar A., Gry C., 1985, ApJ, 298, 838
Fich M., Blitz L., Stark A.A., 1989, ApJ, 342, 272
Frisch P.C., 1995, Space Sci. Rev., 72, 499
Gahm G.F., 1994, Baltic Astron., 3, 85
Gardiner L.T., Noguchi M., 1996, MNRAS, 278, 191
Hartmann D., Burton W.B., 1997, Atlas of Galactic Neutral Hydrogen. Cambridge Univ. Press, Cambridge
Hobbs L.M., 1976, ApJ, 206, L117
Hobbs L.M., Wallerstein G., Hu E.M., 1982, ApJ, 252, L17
Hobbs L.M., Vidal-Madjar A., Ferlet R., Albert C.E., Gry C., 1985, ApJ, 293, L29
Holweger H., Hempel M., Kamp I., 1999, A&A, 350, 603
Houk N., Smith-Moore M., 1988, Michigan Catalogue of Two-Dimensional Spectral Types for the HD Stars, Vol. 4. Univ. of Michigan, Ann Arbor
Howarth I.D., Murray J., Mills D., Berry D.S., 1998, Starlink User Note, 50.21
Hulsbosch A.N.M., Wakker B.P., 1988, A&AS, 75, 191
Jura M., 1976, ApJ, 206, 691
Kalberla P.M.W., Westphalen G., Pietz J., Mebold U., Hartmann D., Burton W.B., 1997, in Lesch H., Dettmar R.-J., Mebold U., Schlickeiser R., eds, The Physics of Galactic Halos. Akademie Verlag, Berlin, p. 57
Lallement R., Bertin P., Chassefiere E., Scott N., 1993, A&A, 271, 734
Large M.I., Quigley M.J.S., Haslam C.G.T., 1962, MNRAS, 124, 405
Lesh J.R., 1968, ApJS, 17, 371
Lockman F.J., 1984, ApJ, 283, 90
Lockman F.J., Gehman C.S., 1991, ApJ, 382, 182
Lockman F.J., Hobbs L.M., Shull J.M., 1986, ApJ, 301, 380
Morras R., Bajaja E., Pöppel W.G.I., 2000, A&AS, 142, 25
Morton D.C., 1991, ApJS, 77, 119
Münch G., 1957, ApJ, 125, 42
Phillips A.P., Pettini M., Gondhalekar P.M., 1984, MNRAS, 206, 337
Pottasch S.R., 1972, A&A, 20, 245
Reynolds R.J., 1997, in Lesch H., Dettmar R.-J., Mebold U., Schlickeiser R., eds, The Physics of Galactic Halos. Akademie Verlag, Berlin, p. 57
Routly P.M., Spitzer L., 1952, ApJ, 115, 227
Savage B., Sembach K., 1996, ApJ, 457, 211
Schmidt-Kaler T.H., 1982, in Schaifers K., Voigt H.H., eds, Landolt-Börnstein, Numerical Data and Functional Relationships in Science and Technology. Group VI, Astronomy, Astrophysics and Space Research, Vol. 2b. Springer-Verlag, Berlin
Sfeir D.M., Lallement R., Crifo F., Welsh B.Y., 1999, A&A, 346, 785
Shapiro P.R., Field G.B., 1976, ApJ, 205, 762
Shaw C.R., Bates B., Kemp S.N., Keenan F.P., Davies R.D., Roger R.S., 1996, ApJ, 473, 849
Shortridge K. et al., 1998, Starlink User Note, 86.16
Siluk R.S., Silk J., 1974, ApJ, 192, 51
Smith K.C., 1992, PhD thesis, Univ. London
Spitzer L., 1990, ARA&A, 28, 71
Spitzer L., Fitzpatrick E.L., 1993, ApJ, 409, 299
Vallée J.P., 1994, A&SS, 220, 243
Vallerga J.V., Vedder P.W., Craig N., Welsh B.Y., 1993, ApJ, 411, 729
Wakker B.P., 2001, ApJS, 136, 463
Wakker B.P., Mathis J.S., 2000, ApJ, 544, L107
Wakker B.P., van Woerden H., 1991, A&A, 250, 509
Wakker B.P., van Woerden H., 1997, ARA&A, 35, 217
Welsh B.Y., Sfeir D.M., Sirk M.M., Lallement R., 1999, A&A, 352, 308
Welty D.E., Hobbs L.M., Kulkarni V.P., 1994, ApJ, 436, 152
Welty D.E., Morton D.C., Hobbs L.M., 1996, ApJS, 106, 533
White R.E., 1974, A&A, 31, 459

This paper has been typeset from a TEX/LATEX file prepared by the author.

Downloaded from https://academic.oup.com/mnras/article-abstract/337/2/720/1026619 by Birkbeck College, University of London user on 12 August 2019